Am J Cancer Res 2021;11(1):108-122
www.ajcr.us /ISSN:2156-6976/ajcr0118824

Original Article

A circGLIS3/miR-644a/PTBP1 positive feedback loop promotes the malignant biological progressions of non-small cell lung cancer

Zhixiong Wu*, Hong Jiang*, Hong Fu, Yan Zhang

*Department of Oncology, Tongji Hospital of Tongji University, Shanghai, China. *Equal contributors.*

Received July 23, 2020; Accepted November 16, 2020; Epub January 1, 2021; Published January 15, 2021

Abstract: Non-small cell lung cancer (NSCLC) is a severe cancer which critically threatens human health in the world. Circular RNAs (circRNAs) are non-coding RNAs that involve in cancer progression. We want to explore the roles of circRNAs in NSCLC in this study. In current study, circGLIS3 was found to be highly expressed in NSCLC tissues and cell lines and high circGLIS3 level was correlated to malignant characteristics and poor prognosis of NSCLC. Functional experiments suggested that circGLIS3 promoted proliferation, migration and invasion and arrested apoptosis of NSCLC cells in vitro. CircGLIS3 also participated in the in vivo process by accelerate NSCLC tumor growth and metastasis. Mechanistically, circGLIS3 could sponging multiple anti-cancer miRNAs including miR-526b, miR-198, miR-498 and miR-664a. Here, we for the first time confirmed that miR-644a was downregulated and functioned as a tumor suppression gene in NSCLC. In addition, we found PTBP1 as a novel target of miR-644a and circGLIS3 could raise the expression of PTBP1 via miR-644a. And PTBP1 could bind to the flanking introns of circGLIS3 and thereby promoting looping of circGLIS3. In conclusion, CircGLIS3 functions as an oncogene via sponging multiple tumor-suppressive miRNAs in NSCLC. A circGLIS3/miR-644a/PTBP1 positive feedback loop exists in the tumorigenesis and development of NSCLC.

Keywords: Non-small cell lung cancer, Circular RNA, miRNA, PTBP1

Introduction

Lung cancer is the leading cause of cancer-related deaths worldwide and non-small cell lung cancer (NSCLC) accounts for up to 85% of all lung cancer cases [1, 2]. Although great progresses have been achieved in the diagnosis and treatments for NSCLC, the 5-year overall survival rate of NSCLC patients still remains low [3]. Many molecules have been discovered to involve in the malignant process of NSCLC which jointly cause poor prognosis of NSCLC [4]. Therefore, it is of clinical significance to understand the roles and mechanisms of these molecules for designing effective therapeutic targets.

Circular RNAs (circRNAs), a novel class of non-coding RNA, are marked by its covalently closed loop without 5' to 3' polarity or polyadenylated tail [5]. Increasing evidences have demonstrated that circRNAs are differentially expressed in various diseases and play important roles in the progression of these diseases, especially cancers [6, 7]. Recently, multiple circRNAs have been uncovered to be involved in the tumorigenesis of NSCLC, indicating that circRNAs are novel molecular regulators in NSCLC [8-10]. However, the roles of most circRNAs in NSCLC remains unclear and require further explorations.

Here, we identified a significantly up-regulated circRNA, circGLIS3 (hsa_circ_0004221), in NSCLC from the human circular RNA microarray data of a published study [11]. CircGLIS3 was derived from the exons 5, 6, 7 and 8 of the GLIS3 gene. Previous studies have shown that GLIS3 gene are closely related to the occurrence and progression of a variety of human cancers [12-14]. However, the roles and mechanisms of circGLIS3 in cancers have not been reported. Then, we intended to verify the expressions of circGLIS3 in NSCLC tissues and

Table 1. Correlation between the clinical data of NSCLC patients with circGLIS3 or miR-644a expression

Clinical data	N	circGLIS3 high	circGLIS3 low	*P*	miR-644a high	miR-644a low	*P*
Gender							
Male	48	23	25		27	21	
Female	32	17	15	0.648	13	19	0.171
Age							
< 65 y	53	26	27		29	24	
≥ 65 y	27	14	13	0.813	11	16	0.237
Tumor size							
< 3 cm	46	16	30		27	19	
≥ 3 cm	34	24	10	0.002	13	21	0.070
Lymph node metastasis							
No	56	21	35		33	23	
Yes	24	19	5	0.001	7	17	0.015
Differentiation							
Well	31	18	13		14	17	
Moderate/Poor	49	22	27	0.251	26	23	0.491
TNM stage							
I-II	55	21	34		32	23	
III-IV	25	19	6	0.002	8	17	0.030

Low and High expression group were divided according to the median of relative RNA expressions; data were analyzed by Chi-square test.

cell lines and investigate the biological functions and mechanisms in vitro and in vivo in NSCLC.

Materials and methods

Tissue samples

A total of 80 human NSCLC tissues and 80 paired adjacent normal lung tissues were collected from NSCLC patients who underwent surgical resection at the Tongji Hospital of Tongji University. None of the patients received radiochemotherapy before surgery. Written informed consents were signed by all the patients and this study was approved by the ethics committee of Tongji Hospital of Tongji University. The clinical features of the patients are shown in **Table 1**.

Cell culture and transfection

NSCLC cell lines, including A549, PC-9, H1299, H460, H1650, and human bronchial epithelial cells (HBE) were all obtained from the type Culture Collection of Chinese Academy of Sciences (Shanghai, China) and cultured in RPMI 1640 medium (HyClone, Utah, USA) supplemented with 10% fetal bovine serum (FBS) at 37°C in a humidified atmosphere with 5% CO_2. Plasmids and oligonucleotides transfection was performed using Lipofectamine 3000 (Invitrogen, CA, USA). CircGLIS3 overexpression plasmids were constructed by inserting the sequence into a pcDNA3.1 (+) CircRNA Mini vector (Addgene, MA, USA). The target sequences of circGLIS3 shRNAs were presented in **Table 2**.

RNA preparation and quantitative real-time PCR (qRT-PCR)

TRIzol (Invitrogen) was used to extract total RNAs from NSCLC tissues and cell lines. Nuclear and cytoplasmic RNAs were separated using PARIS Kit (Invitrogen). RNAs were reverse transcribed by a Prime Script RT Master Mix (Takara, Dalian, China) and analyzed by qPCR assays with SYBR Green PCR Kit (Takara). miRNAs expressions were detected using Hairpin-itTM Quantitation PCR Kit (GenePharma, Shanghai, China). GAPDH and U6 were selected as internal control. RNA expressions were quantified by the $2^{-\Delta\Delta Ct}$ method. The back-

Table 2. Oligonucleotides sequences used in this study

Oligonucleotides	Sequence (5'-3')
Target site of circGLIS3 shRNA#1	ACGCAGGAGCUGAGAGUUUGA
Target site of circGLIS3 shRNA#2	AGGAGCUGAGAGUUUGAAGGU
Target site of circGLIS3 shRNA#3	GGAGCUGAGAGUUUGAAGGUU
circGLIS3 primers	Forward: CAGGAGCTGAGAGTTTGAAGGT
	Reverse: CGGATGCTGGCACAAATACG
linear-GLIS3 primers	Forward: TCAAGCCGAAGTGGAACAGC
	Reverse: TGGAGGTAACTGGGAGGAGG
GAPDH primers	Forward: CAATGACCCCTTCATTGACC
	Reverse: TTGATTTTGGAGGGATCTCG
divergent-GAPDH primers	Forward: GAAGGTGAAGGTCGAGTC
	Reverse: GAAGATGGTGATGGGATTTC

splicing junction site in the PCR products was validated by Sanger sequencing. The existence of circGLIS3 was validated in A549 and H1299 cell lines by RT-PCR conducted with divergent primers. The primers were presented in **Table 2**.

RNA fluorescence in situ hybridization (RNA-FISH)

RNA-FISH assay was conducted using a FISH Tag™ RNA Green Kit (Thermo Scientific, MA, USA) and a biotin-labeled probes specific to circGLIS3 back-splice region. Cell nucleus were counterstained with 4,6-diamidino-2-phenylindole (DAPI). The images were captured with a confocal microscope (Olympus, Tokyo, Japan).

In vitro proliferation, apoptosis, migration and invasion assays

Cell proliferation was assessed using a EdU Cell Proliferation Assay (Sigma-Aldrich, MO, USA) and the EdU positive rates represented the relative proliferation ability of cells. Cell apoptosis rates were detected using Annexin V-FITC/PI Apoptosis Kit (Abnova, Taipei, Taiwan) and flow cytometry. Cell migration capacity was evaluated by a wound-healing assay and the would-healing rate was used to evaluate cell migration ability. Cell invasion capability was measured by a transwell assay and the stained cells invading through the membrane represented the relative invasion capability of cells.

In vivo xenograft assays

The circGLIS3 shRNA#1 or pri-miR-644a was packed by a lentiviral vector and stably transfected into A549 cells. To assess tumor growth, the cells (1×10^6, 100 μL) were subcutaneously injected into five male BALB/c mice (6 weeks). After two weeks, tumors were resected and tumor sizes were measured to calculate the tumor volumes. To assess tumor migration, cells (3×10^6 cells) were intravenously injected into the tail vein of five male BALB/c mice. After 40 days, the mice were sacrificed and their lungs were subjected to H&E staining to identify metastatic lesions. This animal study was approved by the ethics committee of Tongji Hospital of Tongji University.

RNA pull-down assay

For the circRNA-miRNA interaction, RNA pull-down assay was performed using the biotin-labeled probes specific to circGLIS3 back-splice region and streptavidin magnetic beads (Life Technologies, CA, USA). The pulled-down materials were then subjected to Trizol reagent to isolate RNAs. The abundances of predicted miRNAs were analyzed by qRT-PCR assay.

For the RNA binding protein (RBP)-intron interaction, the introns RNAs were obtained using in vitro transcription by T7 RNA polymerase (Ambion Life, MA, USA) and purified by RNeasy Plus Mini Kit (QIAGEN, CA, USA). The RNAs were biotin-labeled using Biotin RNA Labeling Mix (Ambion Life). Then, the biotin-labeled RNAs and Streptavidin magnetic beads (Life Technologies) were used to conduct the pull-down assays. The proteins pulled-down were analyzed by western blot assay.

Dual-luciferase reporter assay

The sequence of circGLIS3 or PTBP1 3'UTR containing miRNAs binding sites, including wild-type and mutant-type, were synthesized and inserted into a pmirGLO vector (Promega, WI, USA). The luciferase reporters were co-transfected with miRNA mimics into A549 cells for 48 hours. The luciferase activities were tested using a dual-luciferase reporter assay system (Promega).

Western blot assay

Total protein was extracted from cells using RIPA Lysis Buffer. Proteins were separated by SDS-PAGE gel and transferred onto a PVDF membrane. The membrane was incubated with primary antibodies (anti-PTBP1, ab30317 and anti-GAPDH, ab8245, Abcam, MA, USA) and HRP-labeled secondary antibody. Images were detected using an enhanced chemiluminescence (ECL) substrate kit (Invitrogen).

Immunofluorescence

Cells were fixed with 4% paraformaldehyde and incubated with anti-PTBP1 antibody (ab30317, Abcam) overnight at 4°C. Then, cells were incubated with mouse anti-goat IgG/FITC antibody for 2 h at room temperature. Cell nucleus were counterstained with DAPI. The images were captured with a confocal microscope (Olympus).

Statistical analyses

Statistical analyses were performed with SPSS 19.0 software (SPSS, IL, USA). Data are presented as the mean ± standard deviation (SD). The Chi-square test or Pearson's Correlation analysis was used to analyze the correlations. Student's t test or one-way analysis of variance was applied to assess comparison across groups. *P*-value < 0.05 was considered statistically significant.

Results

Identification of circGLIS3 in NSCLC

First, we identified that circGLIS3 was originated from exons 5, 6, 7 and 8 of the GLIS3 gene (**Figure 1A**). Then, divergent primers were designed to detect circGLIS3 and PCR assays displayed that divergent primers only amplified circGLIS3 in cDNA but not in genomic DNA (gDNA), while convergent primers amplified the linear GLIS3 in both cDNA and gDNA (**Figure 1B**). The back-splicing junction site of exon 8 toward exon 5 in PCR products generated with divergent primers was also verified by the Sanger sequencing (**Figure 1C**). To explore the circGLIS3 expression in NSCLC, qRT-PCR assay and divergent primers were applied to measure its expression in NSCLC tissues and cell lines. The results showed that circGLIS3 was highly expressed in NSCLC tissues and cell lines (**Figure 1D** and **1E**). We also found that high circGLIS3 level was correlated with larger tumor size, lymphatic metastasis, later TNM stage (**Table 1**) and shorter overall survival time (**Figure 1F**) of NSCLC patients.

CircGLIS3 promotes NSCLC progression in vitro and in vivo

To explore the biological functions of circGLIS3 in NSCLC, circGLIS3 expression plasmids were transfected into H1299 cells (**Figure 2A**) and circGLIS3 shRNAs were transfected into A549 cells (**Figure 2B**). Then, EdU assays suggested that overexpression of circGLIS3 promoted proliferation of H1299 cells and silencing of circGLIS3 inhibited proliferation of A549 cells (**Figure 2C** and **2D**). Cell apoptosis assays showed that overexpression of circGLIS3 protected H1299 cells from apoptosis and silencing of circGLIS3 accelerated apoptosis of A549 cells (**Figure 2E** and **2F**). Accordingly, would-healing assays (**Figure 2G** and **2H**) and transwell assays (**Figure 2I** and **2J**) uncovered that circGLIS3 facilitated migration and invasion of NSCLC cells. In vivo xenograft assays further validated that tumor growth and metastasis was stagnated after knockdown of circGLIS3 (**Figure 2K** and **2L**). These data all together demonstrated that circGLIS3 promotes NSCLC progression in vitro and in vivo.

CircGLIS3 functions as a sponge for multiple miRNAs in NSCLC cells

Before investigating the mechanisms of circGLIS3 in regulating NSCLC progression, we identified that circGLIS3 was located in both cytoplasm and nucleus of H1299 and A549 cells via FISH assay (**Figure 3A**) and qRT-PCR (**Figure 3B**). Because circGLIS3 is abundant in the cytoplasm, we then examined the role of circGLIS3 in serving as a miRNA sponge. By carrying out RNA pull-down assays, we found miR-644a, miR-526b, miR-198 and miR-498 might bind to circGLIS3 (**Figure 3C**). These miRNAs were verified because they rank the highest scores in binding to circGLIS3 predicted by circular RNA interactome database (https://circinteractome.nia.nih.gov) and showed a tight binding motif of 8mer-1a or 7mer-m8 (**Figure 3D**). Subsequently, these specific binding sites were confirmed by dual-luciferase reporter assays (**Figure 3E-H**). We also presented that miR-644a, the same as circGLIS3, was mainly locat-

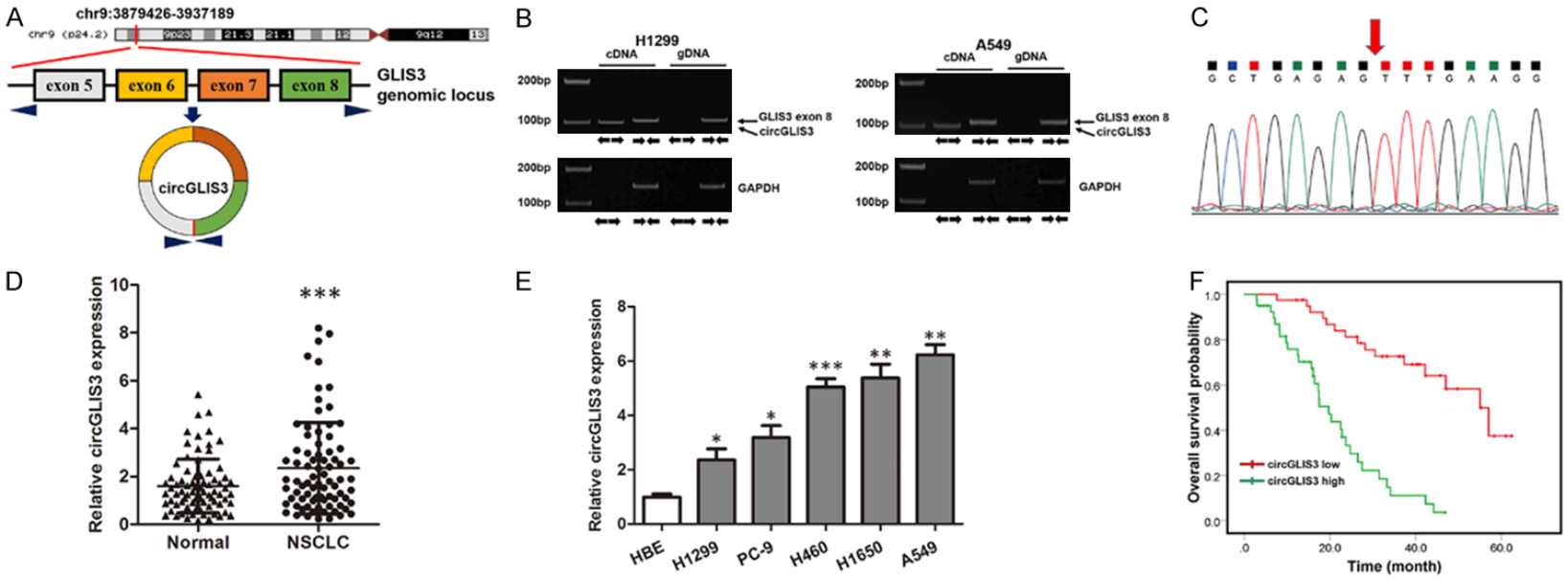

Figure 1. Identification of circGLIS3 in NSCLC. A. Schematic diagram showing the origination of circGLIS3. B. circGLIS3 was amplified by divergent primers only in cDNA but not in gDNA. C. The PCR products were validated by sanger sequencing. D. Comparison of circGLIS3 expression in NSCLC tissues and normal lung tissues. E. Comparison of circGLIS3 expression in NSCLC cell lines and human bronchial epithelial cells. F. Overall survival of NSCLC patients was performed using the Kaplan-Meier method and log-rank test. Data were represented as the mean ± SD, n = 3, $*P < 0.05$, $**P < 0.01$, $***P < 0.001$.

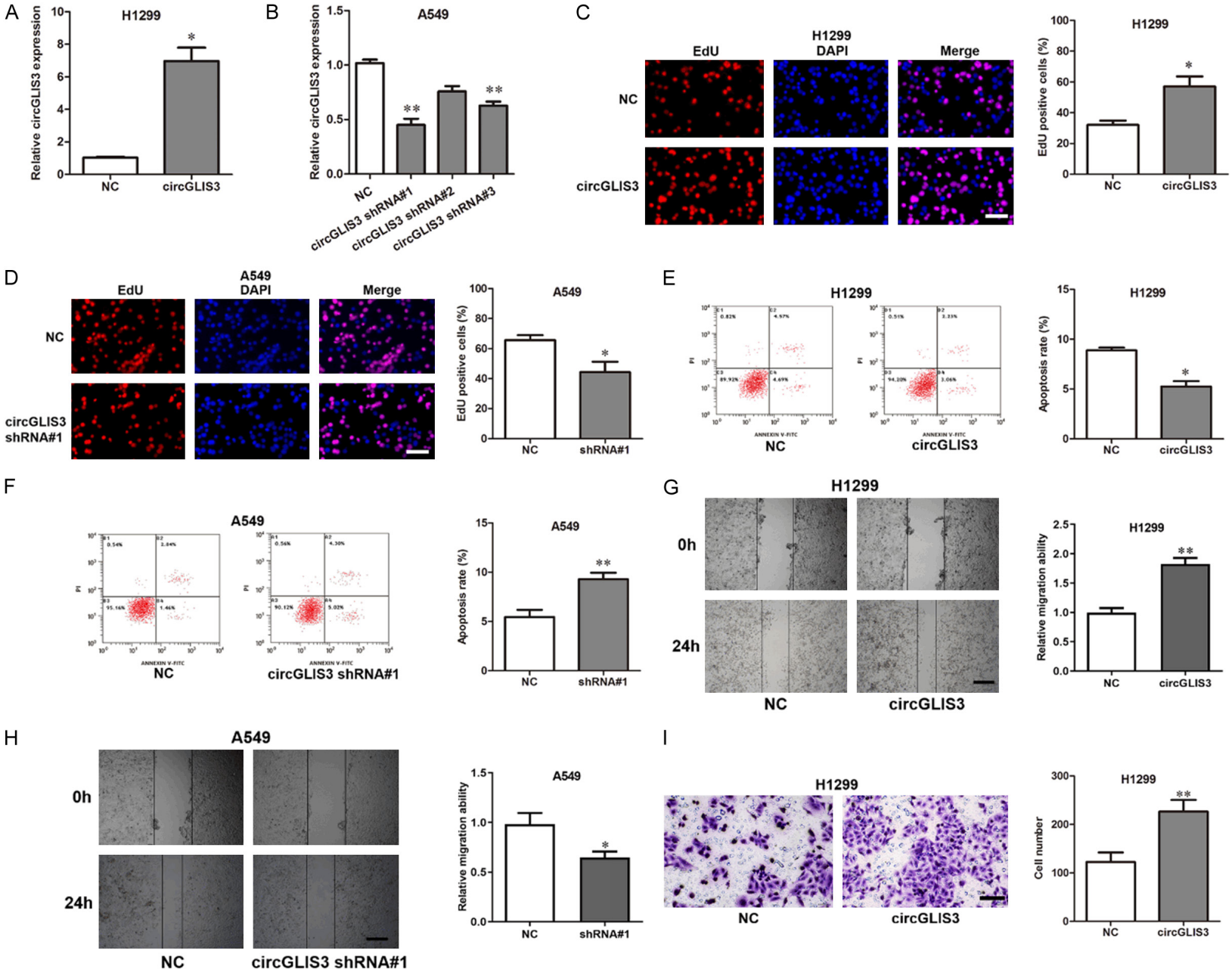
A
H1299
Relative circGLIS3 expression
NC
circGLIS3
B
A549
Relative circGLIS3 expression
NC
circGLIS3 shRNA#1
circGLIS3 shRNA#2
circGLIS3 shRNA#3
C
EdU
H1299
DAPI
Merge
NC
circGLIS3
H1299
EdU positive cells (%)
NC
circGLIS3
D
EdU
A549
DAPI
Merge
NC
circGLIS3 shRNA#1
A549
EdU positive cells (%)
NC
shRNA#1
E
H1299
NC
circGLIS3
H1299
Apoptosis rate (%)
NC
circGLIS3
F
A549
NC
circGLIS3 shRNA#1
A549
Apoptosis rate (%)
NC
shRNA#1
G
H1299
0h
24h
NC
circGLIS3
H1299
Relative migration ability
NC
circGLIS3
H
A549
0h
24h
NC
circGLIS3 shRNA#1
A549
Relative migration ability
NC
shRNA#1
I
H1299
NC
circGLIS3
H1299
Cell number
NC
circGLIS3

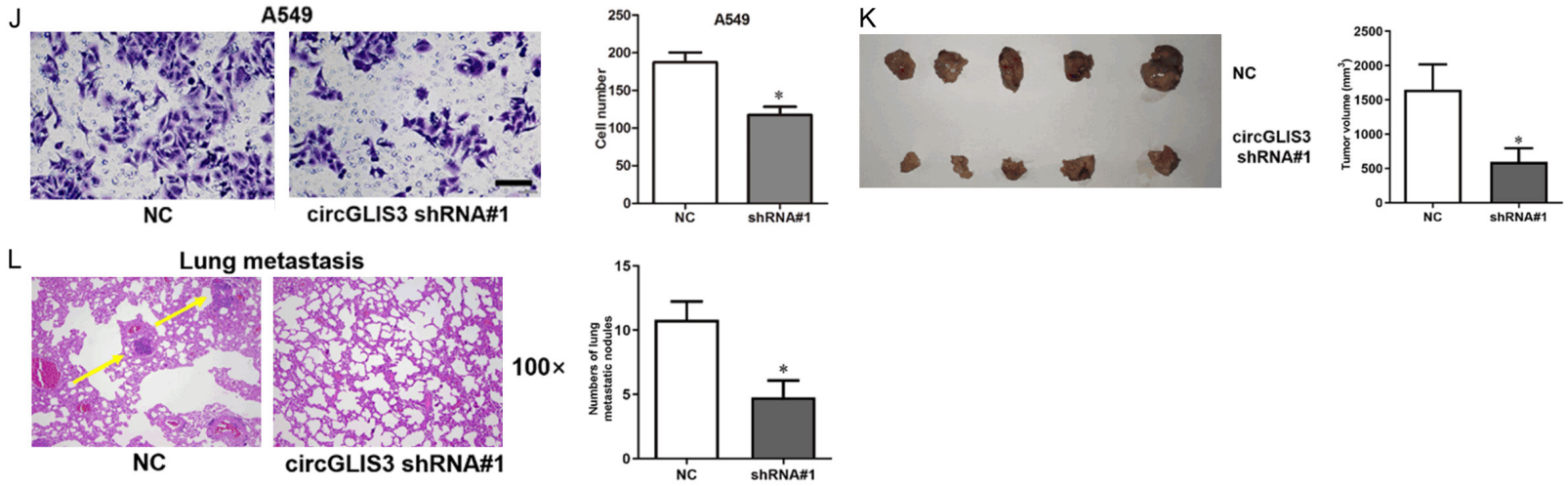

Figure 2. CircGLIS3 promotes NSCLC progression in vitro and in vivo. H1299 cells were transfected with circGLIS3 expression plasmids and A549 cells were transfected with circGLIS3 shRNAs. A, B. circGLIS3 overexpression or silence efficiency was validated by qRT-PCR. C, D. EdU assays were used to assess the proliferation of NSCLC cells; scale bar represents 100 μm. E, F. Flow cytometry assays were applied to detect the apoptosis of NSCLC cells. G, H. Wound-healing assays were carried out to estimate the migration of NSCLC cells; scale bar represents 250 μm. I, J. Transwell assays were performed to appraise the invasion of NSCLC cells; scale bar represents 100 μm. K, L. Xenograft assays assessing the effect of circGLIS3 knockdown on tumor growth and metastasis in vivo. Data were represented as the mean ± SD, n = 3, $*P < 0.05$, $**P < 0.01$.

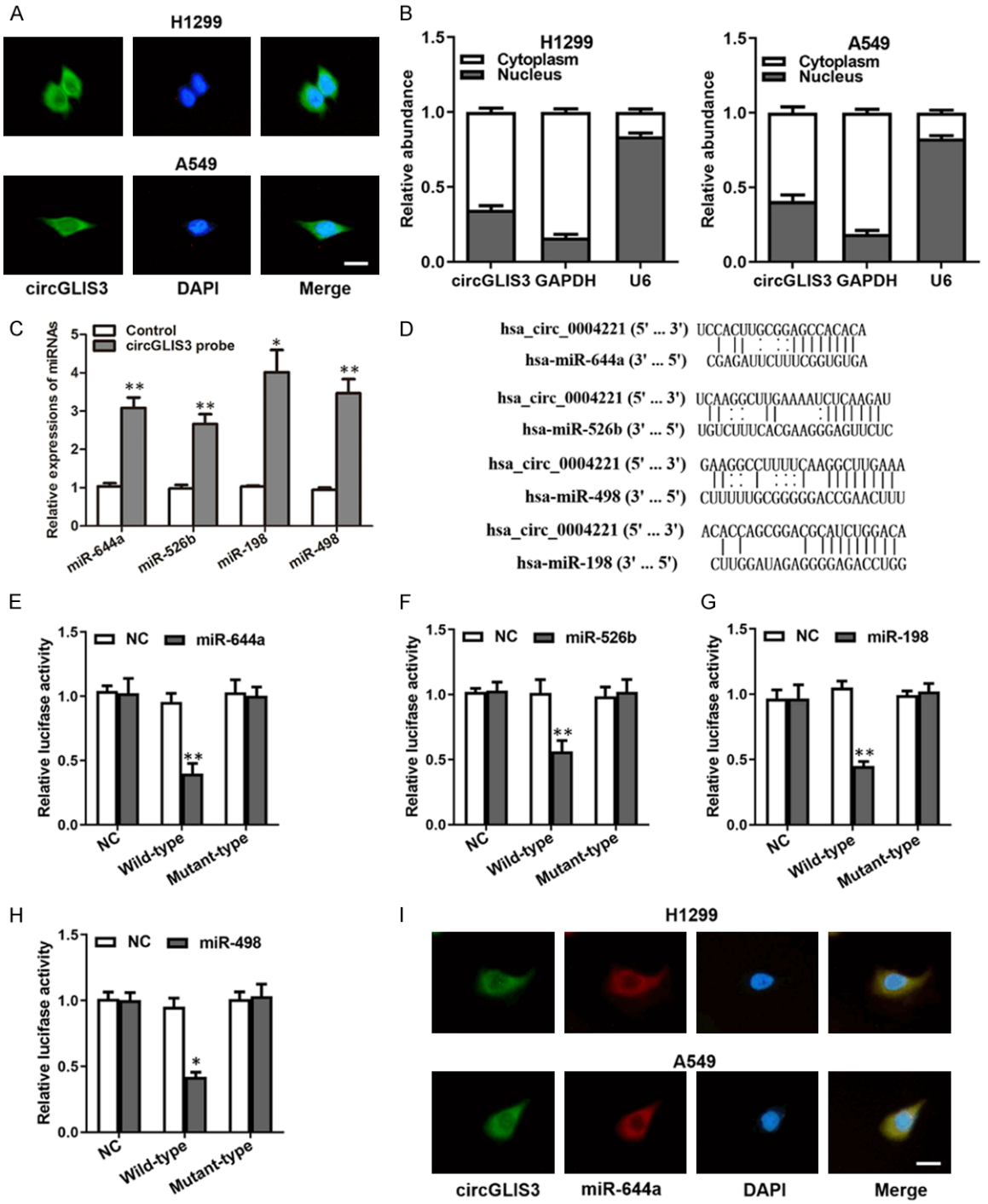

Figure 3. CircGLIS3 functions as a sponge for multiple miRNAs in NSCLC cells. A, B. Subcellular localization of circGLIS3 by FISH and qRT-PCR assays; scale bar represents 20 μm. C. RNA pull-down assay showing the enrichments of miRNAs which could interact with circGLIS3. D. Diagram showing the predicted binding sites of the target miRNAs with circGLIS3. E-H. The predicted target sites were verified by dual-luciferase reporter assays. I. Co-localization of circGLIS3 and miR-644a showed by FISH assay; scale bar represents 20 μm. Data were represented as the mean ± SD, n = 3, $*P < 0.05$, $**P < 0.01$.

ed in the cytoplasm (**Figure 3I**), which was not only the cellular biological basis for its interaction with circGLIS3, but also important basis for binding to target mRNAs. These results sug-

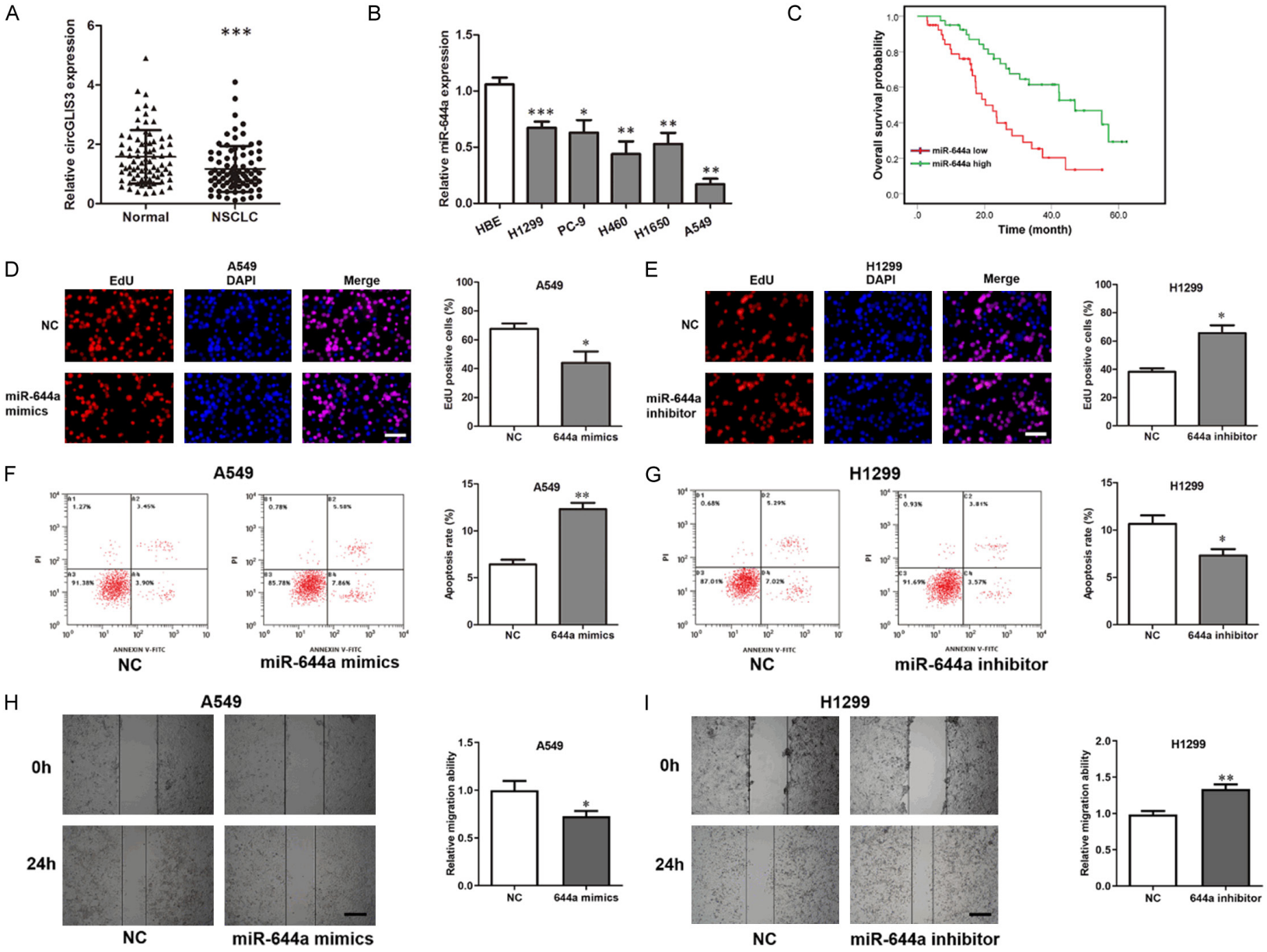
A
Relative circGLIS3 expression
***
Normal
NSCLC
B
Relative miR-644a expression
HBE
H1299
PC-9
H460
H1650
A549
C
Overall survival probability
miR-644a low
miR-644a high
Time (month)
D
EdU
A549
DAPI
Merge
NC
miR-644a mimics
EdU positive cells (%)
644a mimics
E
H1299
miR-644a inhibitor
644a inhibitor
F
Apoptosis rate (%)
ANNEXIN V-FITC
PI
G
H
0h
24h
Relative migration ability
I

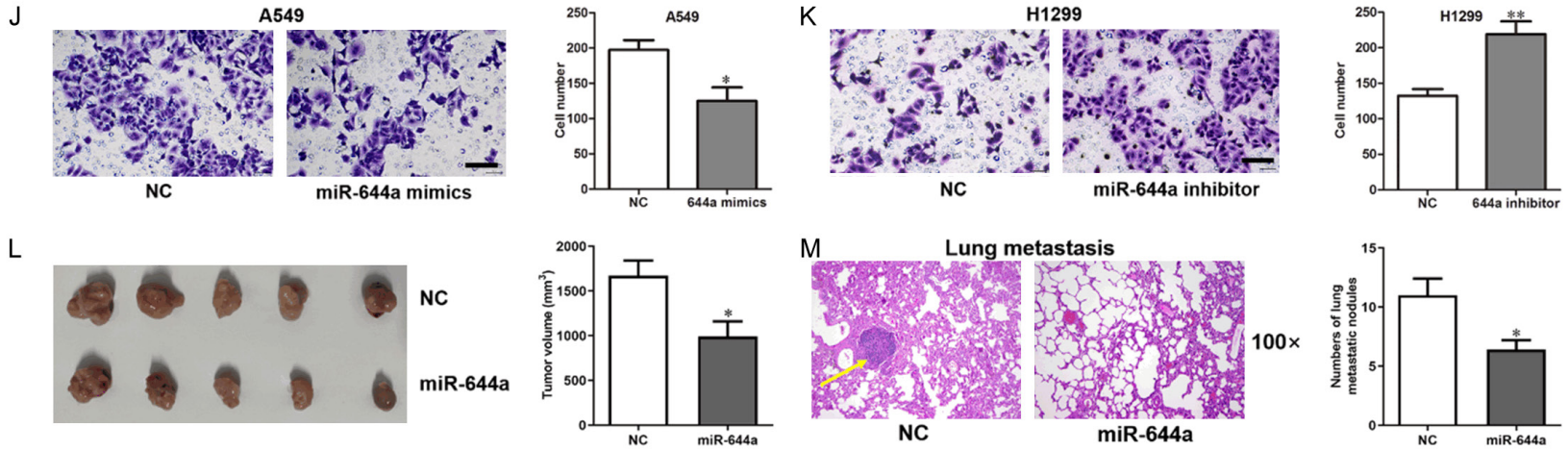

Figure 4. MiR-644 is downregulated and functions as a tumor suppression gene in NSCLC. A. Comparison of miR-644a expression in NSCLC tissues and normal lung tissues. B. Comparison of miR-644a expression in NSCLC cell lines and human bronchial epithelial cells. C. Overall survival of NSCLC patients was performed using the Kaplan-Meier method and log-rank test. D-K. A549 cells were transfected with miR-644a mimics and H1299 cells were transfected with miR-644a inhibitor. D, E. EdU assays were used to assess the proliferation of NSCLC cells; scale bar represents 100 μm. F, G. Flow cytometry assays were applied to detect the apoptosis of NSCLC cells. H, I. Wound-healing assays were carried out to estimate the migration of NSCLC cells; scale bar represents 250 μm. J, K. Transwell assays were performed to appraise the invasion of NSCLC cells; scale bar represents 100 μm. L, M. Xenograft assays assessing the effect of miR-644a overexpression on tumor growth and metastasis in vivo. Data were represented as the mean ± SD, n = 3, $*P < 0.05$, $**P < 0.01$, $***P < 0.001$.

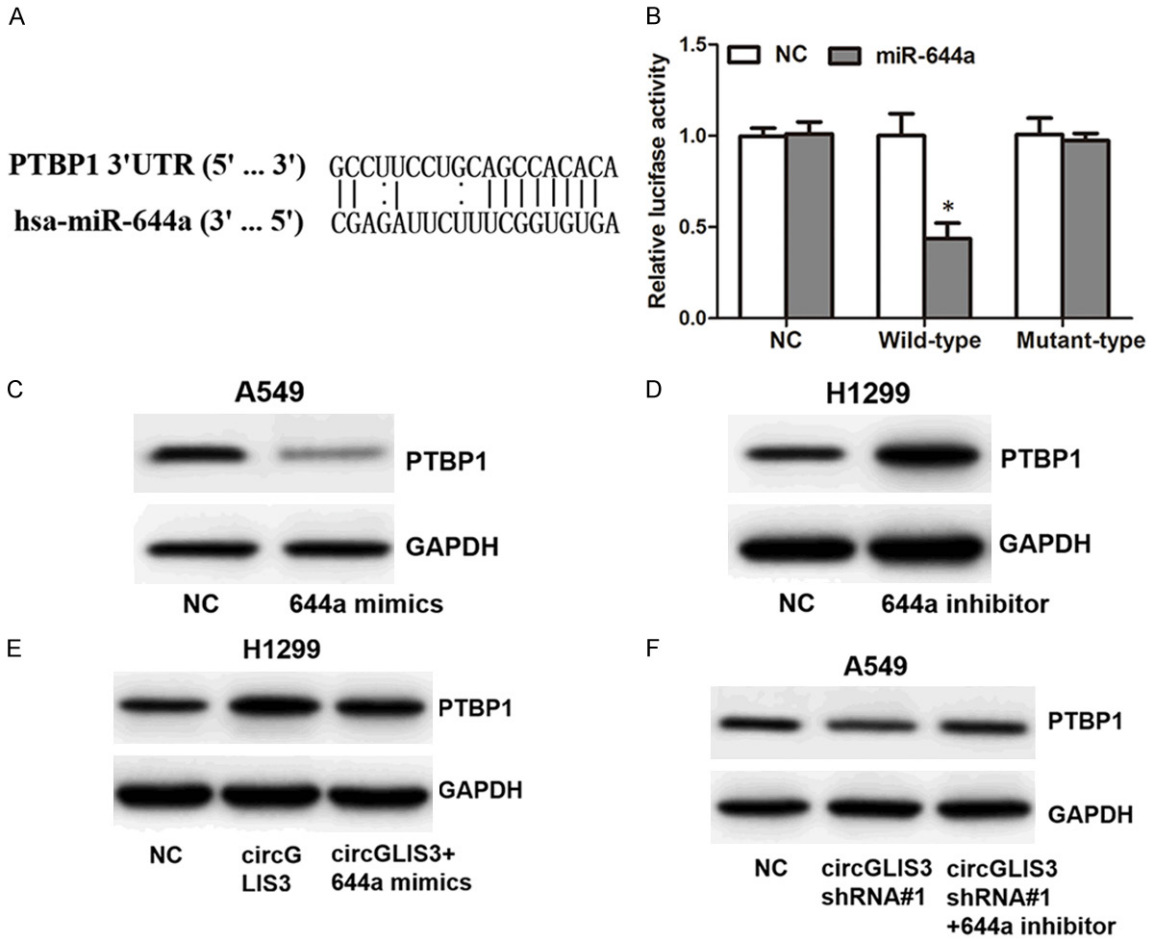

Figure 5. PTBP1 is a target of miR-644a and can be mediated by circGLIS3. A. Diagram showing the predicted binding sites of the miR-644a in PTBP1 3'UTR. B. The predicted target sites were verified by dual-luciferase reporter assays. C, D. Effect of miR-644a on PTBP1 protein expression measured by western blot assays. E, F. Effect of circGLIS3 together with miR-644a on PTBP1 protein expression measured by western blot assays. Data were represented as the mean ± SD, n = 3, $*P < 0.05$.

gested that circGLIS3 functions as a sponge for these miRNAs in NSCLC cells.

MiR-644 is downregulated and functions as a tumor suppression gene in NSCLC

Among the target miRNAs of circGLIS3, miR-526b [15], miR-198 [16] and miR-498 [17] have been reported to be tumor suppression genes in NSCLC, while the roles of miR-644a in NSCLC remains unclear. So, we researched the expressions and functions of miR-644 in NSCLC. We observed that miR-644a expressions were significantly upregulated in NSCLC tissues and cell lines (**Figure 4A** and **4B**). The low expression of miR-644a was found to correlated with TNM stage, lymph node metastasis (**Table 1**) and low overall survival rate (**Figure 4C**). Functional investigations revealed that overexpression of miR-644a restrained proliferation, migration and invasion and expedited apoptosis in A549 cells (**Figure 4D**, **4F**, **4H** and **4J**). Accordingly, silence of miR-644a relieved proliferation, migration and invasion inhibition and arrested apoptosis in A549 cells (**Figure 4E**, **4G**, **4I** and **4K**). In vivo xenograft assays showed that tumor growth and metastasis was stagnated after overexpression of miR-644a (**Figure 4L** and **4M**). So, we concluded that miR-644a was also a tumor suppression gene in NSCLC and circGLIS3 exerted its carcinogenic effects via sponging these carcinostatic miRNAs.

PTBP1 is a target of miR-644a and can be mediated by circGLIS3

Through mircoRNA.org, we identified PTBP1 which serves as an oncogene in many cancers including lung cancer [18-20] as a target

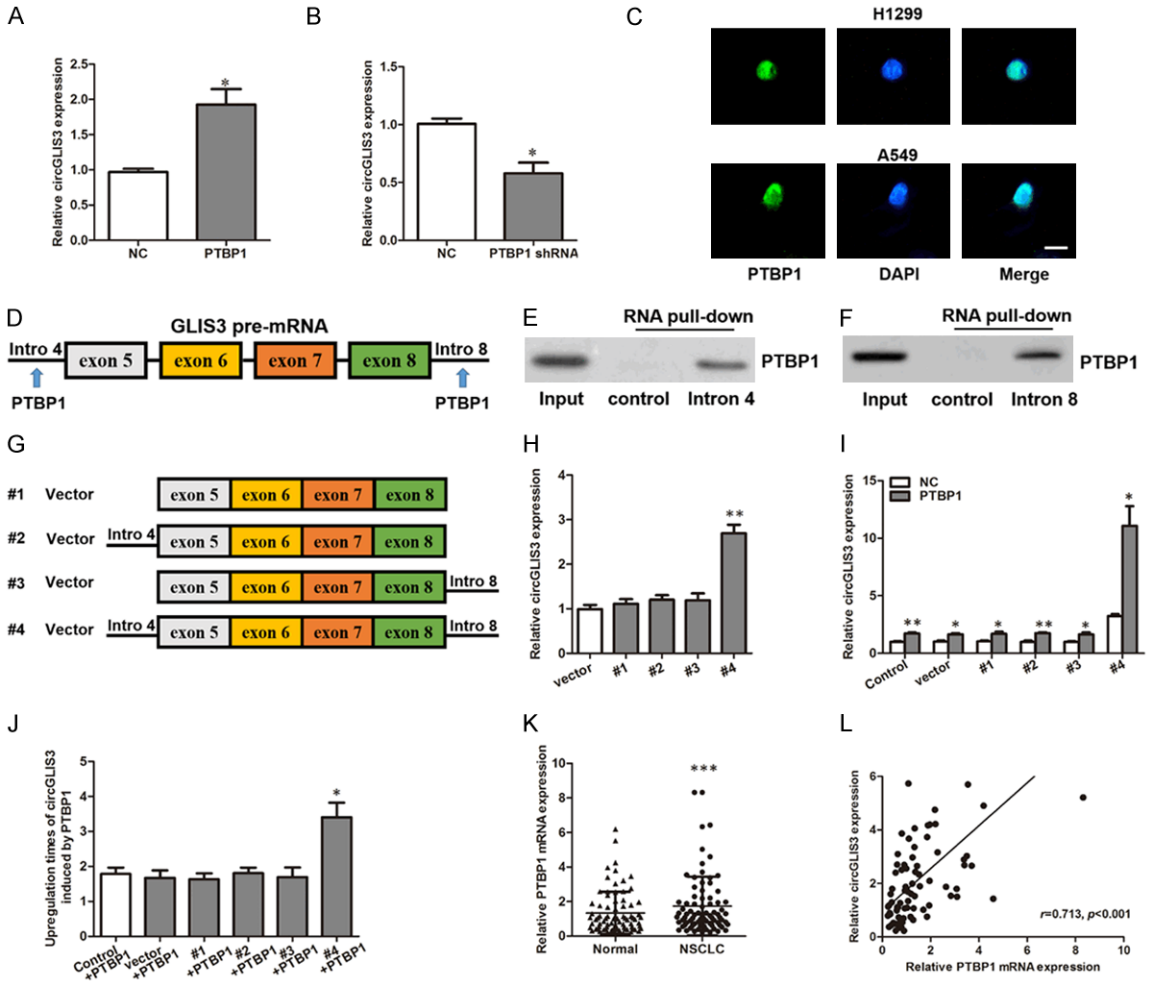

Figure 6. PTBP1 facilitates looping of circGLIS3. A, B. Effect of PTBP1 on circGLIS3 expression measured by qRT-PCR. C. Subcellular localization of PTBP1 protein was detected using immunofluorescence; scale bar represents 20 μm. D. Diagram showing the binding motif of PTBP1 with intron 4 and intron 8 of GLIS3 pre-mRNA. E, F. The binding of PTBP1 with intron 4 and intron 8 of GLIS3 pre-mRNA were verified by RNA pull-down assays. G. Diagram indicated the vectors containing or not containing the flanking introns. H. The vectors were transfected into A549 cells and the expressions of circGLIS3 were detected by qRT-PCR. I. The vectors were transfected into A549 cells together with PTBP1 expression plasmid and the expressions of circGLIS3 were detected by qRT-PCR. J. Comparison of the upregulation times of circGLIS3 induced by PTBP1 after A549 cells were transfected with different vectors. K. Comparison of PTBP1 mRNA expressions in NSCLC tissues and normal lung tissues. L. Correlation between PTBP1 mRNA expression and circGLIS3 expression analyzed by Pearson's Correlation analysis. Data were represented as the mean ± SD, n = 3, $*P < 0.05$, $**P < 0.01$, $***P < 0.001$.

of miR-644a (**Figure 5A**). Then, a dual-luciferase reporter assay was carried out to verify the binding site (**Figure 5B**). Additionally, western blot assay showed that overexpressing miR-644a in A549 cells decreased the protein level of PTBP1 (**Figure 5C**) and silencing miR-644a in H1299 cells raised the protein level of PTBP1 (**Figure 5D**). These data indicated that PTBP1 was a target of miR-644a. In addition, we corroborated that circGLIS3 could raise the expression of PTBP1 via miR-644a (**Figure 5E** and **5F**).

PTBP1 facilitates circularization of circGLIS3

Here, we also found that PTBP1 could upregulated the expression of circGLIS3 (**Figure 6A** and **6B**). PTBP1 is able to bind to the polypyrimidine tract of pre-mRNA introns and may promote RNA looping [21]. We also demonstrated that PTBP1 was mainly present in the nucleus of NSCLC cells, which was the indispensable basis for exerting pre-mRNA splicing function (**Figure 6C**). Here, we found that the intron 4 and intron 8 of GLIS3 pre-mRNA con-

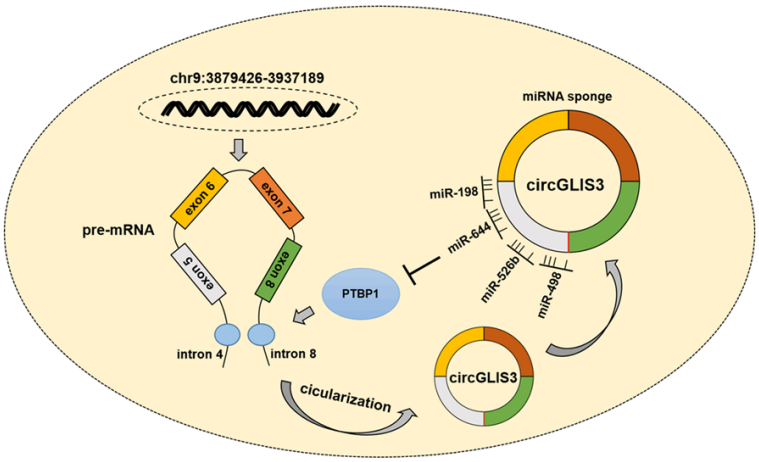

Figure 7. Schematic diagram representing circGLIS3/miR-644a/PTBP1 positive feedback loop in NSCLC development.

tains many PTBP1 binding sites using starBase database (http://starbase.sysu.edu.cn), so we intended to explore how PTBP1 participated in the biogenesis of circGLIS3. To verify these interactions, we performed RNA pull-down assays and observed that PTBP1 could be pulled-down by both intron 4 and intron 8 (**Figure 6D-F**). Then, we constructed several vectors (**Figure 6G**) and transfected them into A549 cells and detected the levels of circGLIS3 by qRT-PCR. The significantly overexpressed circGLIS3 level was detected in cells transfected with vectors containing intron 4 and intron 8 (**Figure 6H**), which implying that the flanking introns participated in the looping of circGLIS3. In addition, A549 cells were transfected with vectors in **Figure 6F** as well as PTBP1 overexpression plasmids. CircGLIS3 expressions were observed upregulated in each group (**Figure 6I**) and the upregulation times of circGLIS3 induced by PTBP1 were then compared. Only cells transfected with vectors containing intron 4 and intron 8 showed higher upregulation times of circGLIS3 than the control group (**Figure 6J**), which indicating that the flanking introns were essential for the circGLIS3 upregulation induce by PTBP1. What's more, we exhibited that PTBP1 mRNA level was increased in NSCLC tissues (**Figure 6K**) and positively correlated to circGLIS3 expression (**Figure 6L**). These results demonstrated that PTBP1 facilitated circGLIS3 expression by binding to the flanking introns and thereby promoting circularization of circGLIS3. In all, we summed up a circGLIS3/miR-644a/PTBP1 positive feedback loop in NSCLC development (**Figure 7**).

Discussion

Nowadays, more and more non-coding RNAs have been revealed to be regulators in the tumorigenesis and development of NSCLC. Herein, we identified a novel circular RNA circGLIS3 and a new miRNA miR-644a differentially expressed in NSCLC. Furthermore, we studied the clinical significances, biological functions and mechanisms of circGLIS3 and miR-644a in NSCLC progression.

First, the highly expressed circGLIS3 was demonstrated to associate with malignant characteristics and poor prognosis of NSCLC, which signifying that it might be a potential biomarker for NSCLC. Afterwards, we revealed that circGLIS3 enhanced NSCLC cellular progression by promoting proliferation, migration and invasion and by preventing apoptosis in vitro. CircGLIS3 also participated in the in vivo process by accelerate NSCLC tumor growth. Thus, we consider circGLIS3 as an oncogene to play a crucial oncogenic role in NSCLC. *In* terms of mechanism, we uncover that circGLIS3 could elaborate its functions via sponging multiple anti-cancer miRNAs including miR-526b, miR-198, miR-498 and miR-664a (which was also proved to be an anti-cancer miRNA subsequently). In summary, circGLIS3 facilitates NSCLC progression by sponging multiple anti-cancer miRNAs.

Up until now, miR-644a has been confirmed to be a tumor suppression gene in some cancers such as castration-resistant prostate cancer [22], hepatocellular carcinoma [23], osteosarcoma [24], gastric cancer [25], breast cancer [26] and esophageal squamous cell carcinoma [27]. However, the expression and roles of miR-644a in NSCLC is still unclear. In this study, miR-644a was found to be downregulated in NSCLC and played an anticarcinogenic function. PTBP1 was identified as a novel target of miR-644a, and its expression can be thereby mediated by circGLIS3. PTBP1 has been reported as an oncogene in many cancers including lung cancer [18-20], hence, we suppose that

circGLIS3 and miR-644a may involve in NSCLC progression via regulating PTBP1.

PTBP1 is a RNA binding protein which plays a role in pre-mRNA splicing. It can bind to the polypyrimidine tract of pre-mRNA introns and may promote RNA looping [21]. A recent study reported that PTBP1 could induce the biosynthesis of circRNA_001160 [28]. Here, we showed that PTBP1 could promoted circGLIS3 expression in NSCLC cells. The mechanism is PTBP1 binding to the flanking introns of circGLIS3 and thereby promoting looping of circGLIS3. There are also some studies report that RNA binding proteins promote circRNA cyclization in the same manner, thus promoting the expression of the circRNAs [29-31]. Since circGLIS3 can raise the expression of PTBP1, we displayed a circGLIS3/miR-644a/PTBP1 positive feedback loop involved in the NSCLC development.

In conclusion, our findings reveal that circGLIS3 functions as an oncogene via sponging multiple tumor-suppressive miRNAs in NSCLC. A circGLIS3/miR-644a/PTBP1 positive feedback loop exists in the tumorigenesis and development of NSCLC.

Acknowledgements

This study was supported by the Fund Project of Shanghai Science and Technology Committee (No. 044119650) and the Foundation of Shanghai Municipal Health Commission (No. 201740038).

Disclosure of conflict of interest

None.

Address correspondence to: Yan Zhang, Department of Oncology, Tongji Hospital of Tongji University, No. 389 Xincun Road, Shanghai 200065, China. Tel: +86-13764188951; E-mail: zhangyan3210233@163.com

References

[1] Hirsch FR, Scagliotti GV, Mulshine JL, Kwon R, Curran WJ, Wu YL and Paz-Ares L. Lung cancer: current therapies and new targeted treatments. Lancet 2017; 389: 299-311.

[2] Relli V, Trerotola M, Guerra E and Alberti S. Abandoning the notion of non-small cell lung cancer. Trends Mol Med 2019; 25: 585-594.

[3] Remon J, Ahn MJ, Girard N, Johnson M, Kim DW, Lopes G, Pillai RN, Solomon B, Villacampa G and Zhou Q. Advanced-stage non-small cell lung cancer: advances in thoracic oncology 2018. J Thorac Oncol 2019; 14: 1134-1155.

[4] Schulze AB, Evers G, Kerkhoff A, Mohr M, Schliemann C, Berdel WE and Schmidt LH. Future options of molecular-targeted therapy in small cell lung cancer. Cancers (Basel) 2019; 11: 690.

[5] Xiao MS, Ai Y and Wilusz JE. Biogenesis and Functions of circular RNAs come into focus. Trends Cell Biol 2020; 30: 226-240.

[6] Han B, Chao J and Yao H. Circular RNA and its mechanisms in disease: from the bench to the clinic. Pharmacol Ther 2018; 187: 31-44.

[7] Zhou R, Wu Y, Wang W, Su W, Liu Y, Wang Y, Fan C, Li X, Li G, Li Y, Xiong W and Zeng Z. Circular RNAs (circRNAs) in cancer. Cancer Lett 2018; 425: 134-142.

[8] Li C, Zhang L, Meng G, Wang Q, Lv X, Zhang J and Li J. Circular RNAs: pivotal molecular regulators and novel diagnostic and prognostic biomarkers in non-small cell lung cancer. J Cancer Res Clin Oncol 2019; 145: 2875-2889.

[9] Li X, Yang B, Ren H, Xiao T, Zhang L, Li L, Li M, Wang X, Zhou H and Zhang W. Hsa_circ_0002483 inhibited the progression and enhanced the Taxol sensitivity of non-small cell lung cancer by targeting miR-182-5p. Cell Death Dis 2019; 10: 953.

[10] Jin M, Shi C, Yang C, Liu J and Huang G. Upregulated circRNA ARHGAP10 predicts an unfavorable prognosis in NSCLC through regulation of the miR-150-5p/GLUT-1 Axis. Mol Ther Nucleic Acids 2019; 18: 219-231.

[11] Jiang MM, Mai ZT, Wan SZ, Chi YM, Zhang X, Sun BH and Di QG. Microarray profiles reveal that circular RNA hsa_circ_0007385 functions as an oncogene in non-small cell lung cancer tumorigenesis. J Cancer Res Clin Oncol 2018; 144: 667-674.

[12] Pinto K and Chetty R. Gene of the month: GLIS1-3. J Clin Pathol 2020; 73: 527-530.

[13] Jetten AM. Emerging roles of GLI-similar krüppel-like zinc finger transcription factors in leukemia and other cancers. Trends Cancer 2019; 5: 547-557.

[14] Chou CK, Tang CJ, Chou HL, Liu CY, Ng MC, Chang YT, Yuan SF, Tsai EM and Chiu CC. The potential role of Krüppel-like zinc-finger protein glis3 in genetic diseases and cancers. Arch Immunol Ther Exp (Warsz) 2017; 65: 381-389.

[15] Zhang ZY, Fu SL, Xu SQ, Zhou X, Liu XS, Xu YJ, Zhao JP and Wei S. By downregulating Ku80, hsa-miR-526b suppresses non-small cell lung cancer. Oncotarget 2015; 6: 1462-77.

[16] Wang S, Zhang X, Yang C and Xu S. MicroRNA-198-5p inhibits the migration and invasion of

non-small lung cancer cells by targeting fucosyltransferase 8. Clin Exp Pharmacol Physiol 2019; 46: 955-967.
[17] Yan R, Jiang Y, Lai B, Lin Y and Wen J. The positive feedback loop FOXO3/CASC11/miR-498 promotes the tumorigenesis of non-small cell lung cancer. Biochem Biophys Res Commun 2019; 519: 518-524.
[18] Zhu W, Zhou BL, Rong LJ, Ye L, Xu HJ, Zhou Y, Yan XJ, Liu WD, Zhu B, Wang L, Jiang XJ and Ren CP. Roles of PTBP1 in alternative splicing, glycolysis, and oncogensis. J Zhejiang Univ Sci B 2020; 21: 122-136.
[19] Cho CY, Chung SY, Lin S, Huang JS, Chen YL, Jiang SS, Cheng LC, Kuo TH, Lay JD, Yang YY, Lai GM and Chuang SE. PTBP1-mediated regulation of AXL mRNA stability plays a role in lung tumorigenesis. Sci Rep 2019; 9: 16922.
[20] Li S, Shen L, Huang L, Lei S, Cai X, Breitzig M, Zhang B, Yang A, Ji W, Huang M, Zheng Q, Sun H and Wang F. PTBP1 enhances exon11a skipping in Mena pre-mRNA to promote migration and invasion in lung carcinoma cells. Biochim Biophys Acta Gene Regul Mech 2019; 1862: 858-869.
[21] Kafasla P, Lin H, Curry S and Jackson RJ. Activation of picornaviral IRESs by PTB shows differential dependence on each PTB RNA-binding domain. RNA 2011; 17: 1120-31.
[22] Ebron JS, Shankar E, Singh J, Sikand K, Weyman CM, Gupta S, Lindner DJ, Liu X, Campbell MJ and Shukla GC. MiR-644a disrupts oncogenic transformation and warburg effect by direct modulation of multiple genes of tumor-promoting pathways. Cancer Res 2019; 79: 1844-1856.
[23] Liang W, Liao Y, Li Z, Wang Y, Zheng S, Xu X, Ran F, Tang B and Wang Z. MicroRNA-644a promotes apoptosis of hepatocellular carcinoma cells by downregulating the expression of heat shock factor 1. Cell Commun Signal 2018; 16: 30.
[24] Sahin Y, Altan Z, Arman K, Bozgeyik E, Koruk Ozer M and Arslan A. Inhibition of miR-664a interferes with the migration of osteosarcoma cells via modulation of MEG3. Biochem Biophys Res Commun 2017; 490: 1100-1105.
[25] Li Y, Yan X, Ren L and Li Y. miR-644a inhibits cellular proliferation and invasion via suppression of CtBP1 in gastric cancer cells. Oncol Res 2018; 26: 1-8.
[26] Raza U, Saatci Ö, Uhlmann S, Ansari SA, Eyüpoğlu E, Yurdusev E, Mutlu M, Ersan PG, Altundağ MK, Zhang JD, Doğan HT, Güler G and Şahin Ö. The miR-644a/CTBP1/p53 axis suppresses drug resistance by simultaneous inhibition of cell survival and epithelial-mesenchymal transition in breast cancer. Oncotarget 2016; 7: 49859-49877.
[27] Zhang JX, Chen ZH, Xu Y, Chen JW, Weng HW, Yun M, Zheng ZS, Chen C, Wu BL, Li EM, Fu JH, Ye S and Xie D. Downregulation of microRNA-644a promotes esophageal squamous cell carcinoma aggressiveness and stem cell-like phenotype via dysregulation of PITX2. Clin Cancer Res 2017; 23: 298-310.
[28] Li H, Shen S, Ruan X, Liu X, Zheng J, Liu Y, Yang C, Wang D, Liu L, Ma J, Ma T, Wang P, Cai H, Li Z, Zhao L and Xue Y. Biosynthetic CircRNA_001160 induced by PTBP1 regulates the permeability of BTB via the CircRNA_001160/miR-195-5p/ETV1 axis. Cell Death Dis 2019; 10: 960.
[29] Ji F, Du R, Chen T, Zhang M, Zhu Y, Luo X and Ding Y. Circular RNA circSLC26A4 accelerates cervical cancer progression via miR-1287-5p/HOXA7 axis. Mol Ther Nucleic Acids 2020; 19: 413-420.
[30] Wang R, Zhang S, Chen X, Li N, Li J, Jia R, Pan Y and Liang H. CircNT5E Acts as a sponge of miR-422a to promote glioblastoma tumorigenesis. Cancer Res 2018; 78: 4812-4825.
[31] Errichelli L, Dini Modigliani S, Laneve P, Colantoni A, Legnini I, Capauto D, Rosa A, De Santis R, Scarfò R, Peruzzi G, Lu L, Caffarelli E, Shneider NA, Morlando M and Bozzoni I. FUS affects circular RNA expression in murine embryonic stem cell-derived motor neurons. Nat Commun 2017; 8: 14741.